

# The origin and tidal evolution of cuspy triaxial haloes

Ben Moore <sup>\*</sup>, Stelios Kazantzidis, Jürg Diemand and Joachim Stadel

*Institute for Theoretical Physics, University of Zürich, CH-8057 Zürich, Switzerland*

## ABSTRACT

We present a technique for constructing equilibrium triaxial  $N$ -body haloes with nearly arbitrary density profiles, axial ratios and spin parameters. The method is based on the way in which structures form in hierarchical cosmological simulations, where prolate and oblate haloes form via mergers with low and high angular momentum respectively. We show that major mergers between equilibrium spherical cuspy haloes produce similarly cuspy triaxial remnants and higher angular momentum mergers produce systems with lower concentrations. Triaxial haloes orbiting within deeper potentials become more spherical and their velocity dispersion tensors more isotropic. Subhaloes within cosmological simulations are significantly rounder than field haloes. The rate of mass loss depends sensitively on the halo shape: a prolate halo can lose mass at a rate several times higher than an isotropic spherical halo with the same density profile.

**Key words:** cosmology: theory – dark matter – galaxies: dynamics and interactions – galaxies: haloes – haloes: evolution – haloes: structure – methods:  $N$ -body simulations.

## 1 INTRODUCTION

A generic prediction of the currently favoured cold dark matter (CDM) cosmological model of hierarchical structure formation is that the dark matter (hereafter DM) haloes of galaxies and clusters are flattened triaxial systems (e.g., Barnes & Efstathiou 1987; Frenk et al. 1988; Dubinski & Carlberg 1991; Warren et al. 1992; Cole & Lacey 1996; Thomas et al. 1998; Jing & Suto 2002). Observationally, inferring the intrinsic shape of DM haloes of galaxies and clusters is a difficult task, but nonetheless several potentially powerful probes exist that may allow us to distinguish between spherical and flattened DM haloes. These include the dynamical modelling of collisionless tracers such as tidal streams orbiting the Milky Way (Johnston et al. 1999; Ibata et al. 2001; Mayer et al. 2002; Majewski et al. 2003; Helmi 2003), the distribution and kinematics of gas in spiral galaxies (Kuijken & Tremaine 1994; Franx, van Gorkom & de Zeeuw 1994; Schoenmakers, Franx & de Zeeuw 1997; Merrifield 2002), and polar ring galaxies (Schweizer, Whitmore & Rubin 1983; Sackett & Sparke 1990; Sparke 2002; Iodice et al. 2003) which provide shape constraints perpendicular to the disc plane, gravitational lensing applications (Kochanek 1995; Bartelmann, Steinmetz & Weiss 1995; Koopmans et al. 1998; Oguri, Lee & Suto 2003) and the flattening of the extended X-ray isophotes in elliptical galaxies (Buote & Canizares 1994, 1996, 1998; Buote et al. 2002).

Numerical experiments of isolated equilibrium models are

very useful for studying the dynamical evolution of gravitating systems in a controlled way. Several techniques exist for constructing  $N$ -body realisations of isolated spherical systems (Hernquist 1993; Kazantzidis, Magorrian & Moore 2003, hereafter KMM), but it is far more complicated to build triaxial equilibria. Even though the Jeans' theorem guarantees that the distribution function depends only on the isolating integrals of motion, explicit expressions for the latter other than the energy per unit mass,  $E$ , are rarely known in the case of triaxial potentials. As a result, the triaxial models that have been constructed so far have been either limited to a few special analytical cases (e.g., Stäckel potentials or rotating  $f(E_J)$  models with  $E_J$  being the Jacobi constant) or entirely based on numerical techniques (Schwarzschild 1979).

Recently, Holley-Bockelmann et al. (2001) used a technique of adiabatically applying a drag to the velocities of the particles along each principal axis in order to create cuspy triaxial systems starting with a spherical Hernquist (Hernquist 1990) model. Also, Boily, Kroupa & Peñarrubia-Garrido (2001) extended the original prescription of Hernquist (1993) to include composite, axisymmetric models of galaxies and haloes by perturbing the velocity field of particles to reflect an imposed potential. These techniques are useful and have been used to understand the response of systems to live triaxial potentials. However, they are somewhat restricted to modest values of the flattening and it is difficult to incorporate a significant amount of rotational flattening.

A general technique for constructing cuspy axisymmetric and triaxial  $N$ -body systems would be advantageous for many purposes including studying the dynamical friction in flattened and rotating systems, the mass loss and tidal stripping from triaxial substructure haloes, the effects of baryonic accretion and disc formation on

<sup>\*</sup> E-mail: moore@physik.unizh.ch (BM); stelios@physik.unizh.ch (SK); diemand@physik.unizh.ch (JD); stadel@physik.unizh.ch (JS)

triaxial halo shape and anisotropy, the effects of triaxial shape on the properties and stability of discs, the interaction between central black holes and cusps and the inflow of gas in triaxial systems. In this paper we present such a technique that is based on the way that haloes in hierarchical models of structure formation obtain their shapes. Inspection of a cosmological simulation reveals that triaxiality arises via mergers that take place with various amounts of angular momentum which is generated from the large scale tidal field. Mergers between two haloes that occur with little angular momentum (radial mergers) produce prolate systems, whilst high angular momentum mergers produce oblate systems. Most CDM haloes form via a sequence of mergers with varying amounts of angular momentum such that haloes with arbitrary triaxiality may be formed and the triaxiality will vary with radius (Moore et al. 2001; Vitvitska et al. 2002).

The outline of this paper is as follows. In Section 2, we describe our technique for constructing equilibrium cuspy  $N$ -body haloes with various degrees of flattening. There we discuss in detail the numerical experiments we performed and present our results for the internal structure of the resulting models. In Section 3, we investigate the tidal evolution of triaxial substructure haloes within a static host potential and study the shape of subhaloes within a cosmological CDM simulation. Finally, we summarise our main results in Section 4.

## 2 CONSTRUCTING CUSPY TRIAXIAL DARK MATTER HALOES

We begin with a cuspy spherical DM halo which follows the Navarro, Frenk & White (1996, hereafter NFW) density profile

$$\rho(r) = \frac{\rho_s}{(r/r_s)(1 + (r/r_s))^2} \quad (r \leq r_{\text{vir}}). \quad (1)$$

Here the characteristic inner density  $\rho_s$  and scale radius  $r_s$ , are sensitive to the epoch of halo formation and tightly correlated with the halo virial parameters, via the concentration,  $c$ , and the virial overdensity  $\Delta_{\text{vir}}$ . Since the NFW density profile corresponds to a cumulative mass distribution that diverges as  $r \rightarrow \infty$ , we implement an exponential cut-off for  $r > r_{\text{vir}}$  which sets in at the virial radius and turns off the profile on a scale  $r_{\text{decay}}$  which is a free parameter and controls the sharpness of the transition

$$\rho(r) = \frac{\rho_s}{c(1+c)^2} \left( \frac{r}{r_{\text{vir}}} \right)^\epsilon \exp \left[ -\frac{r - r_{\text{vir}}}{r_{\text{decay}}} \right] \quad (r > r_{\text{vir}}), \quad (2)$$

where  $c \equiv r_{\text{vir}}/r_s$  is the concentration parameter. Finally, in order to ensure a smooth transition between (1) and (2) at  $r_{\text{vir}}$ , we require the logarithmic slope there to be continuous. This implies

$$\epsilon = -\frac{1+3c}{1+c} + \frac{r_{\text{vir}}}{r_{\text{decay}}}. \quad (3)$$

Once the density profile  $\rho(r)$  of our initial model has been specified, we construct an  $N$ -body realisation using the technique discussed in detail in KMM. To summarise, the particle positions and velocities are initialised by sampling the exact phase-space distribution function using Eddington's inversion formula (Eddington 1916) for the given density profile  $\rho(r)$  and assuming spherical symmetry. Note that in this paper we will consider only initial models with isotropic velocity dispersion tensors and therefore their distribution function will only depend on the binding energy  $E$ ,  $f = f(E)$ . For the following experiments we begin with an initial galaxy-sized halo with virial mass  $M_{\text{vir}} = 7 \times 10^{11} h^{-1} M_\odot$

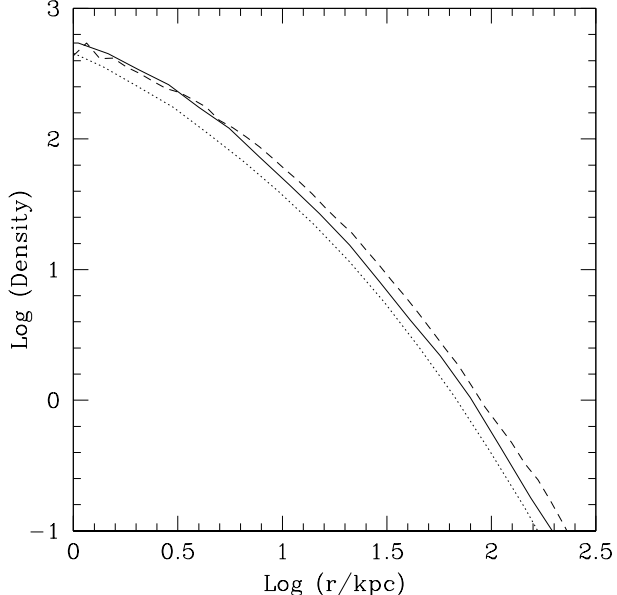


**Figure 1.** The spherically averaged density profiles of the initial model (dotted curve), the  $a:b:c = 2:1:1$  prolate model (solid curve) and the  $a:b:c = 2:2:1$  oblate model (dashed curve).

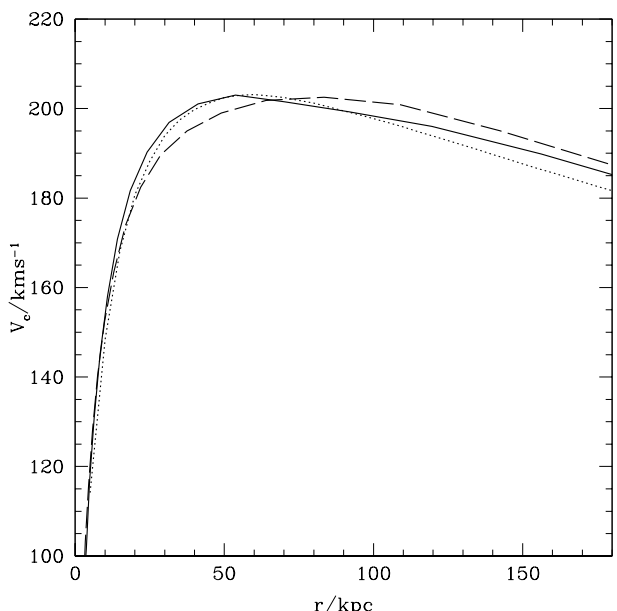


**Figure 2.** Circular velocity curves ( $V_c = \sqrt{GM/r}$ ) scaled to the same peak circular velocity, for the initial model (dotted), prolate  $a:b:c = 2:1:1$  halo (solid) and oblate  $a:b:c = 2:2:1$  halo (dashed).

and concentration of  $c = 10$  in accordance with theoretical predictions for objects at this mass scale and for the adopted cosmology (e.g., Bullock et al. 2001). Note that for all simulations presented in this paper including the cosmological ones described in the next section, we consider as our framework the concordance flat  $\Lambda$ CDM model with present-day matter and vacuum densities  $\Omega_m = 0.3$  and  $\Omega_\Lambda = 0.7$  respectively, dimensionless Hubble constant  $h = 0.7$ , present-day fluctuation amplitude  $\sigma_8 = 0.9$  and index of the primordial power spectrum  $n = 1.0$ . For the latter choice of concentration, the virial and scale radius of the initial halo model

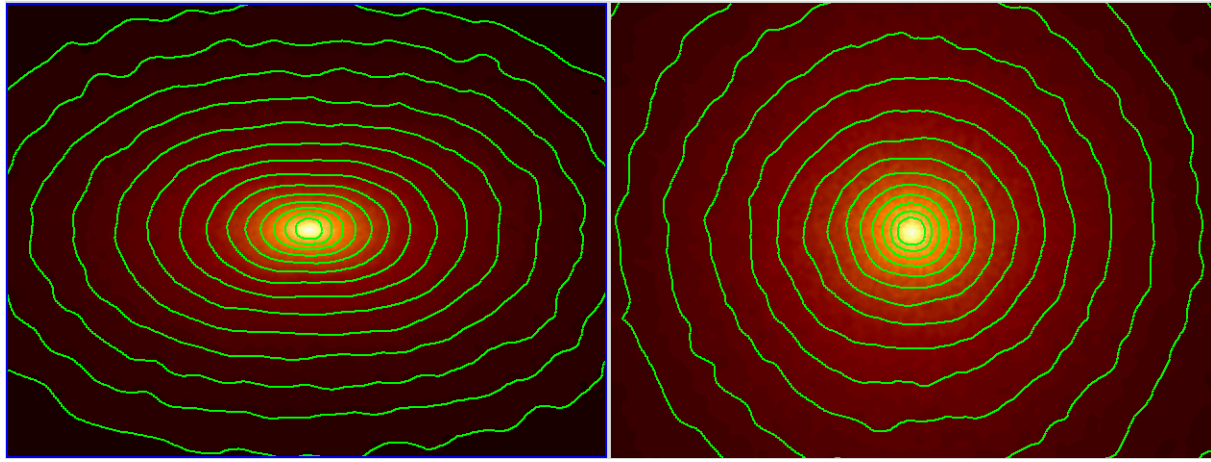


**Figure 3.** Logarithmically spaced surface density contours of the oblate model viewed in the plane of the long axis (left) and short axis (right).

are  $r_{\text{vir}} = 181 h^{-1}$  kpc and  $r_s = 18.1 h^{-1}$  kpc, respectively. The initial model is constructed with  $N = 5 \times 10^5$  particles and we use a gravitational softening of  $\epsilon = 0.3 h^{-1}$  kpc.

All the simulations presented in this paper were carried out using PKDGRAV, a multi-stepping, parallel  $N$ -body code (Stadel 2001) which uses a spline kernel softening and multi-stepping based on the local acceleration of particles. The time integration was performed with high enough accuracy such that the total energy was conserved to better than 0.1% in all cases. We have also explicitly checked that our results are not compromised by choices of force softening, time-stepping or opening angle criteria in the treecode.

We perform a first experiment in which we merge two identical spherical haloes with zero angular momentum corresponding to a head-on collision with an impact parameter  $b = 0$ . The initial relative separation of the two haloes is  $r_{\text{sep}} = 300$  kpc and are they infalling at a relative speed of  $v_{\text{rel}} = 300$  km s $^{-1}$ . Relative velocities significantly higher than the latter value lead to unbound orbits, so we chose this value so as to maximize the amount of flattening from a single merger. Note that the initial separation corresponds to haloes which are overlapping. This does not influence the final result as nearly identical remnants were produced with non-overlapping initial models. The two haloes merge within a time-scale of order the crossing time  $t_{\text{cross}} = \sqrt{r_{\text{vir}}^3/GM_{\text{vir}}}$  which is approximately equal to 2 Gyr for our initial models. In all simulations the merger remnants were allowed to settle into equilibrium for several crossing times after the merger was complete which was established by monitoring the fluctuations of the density profile of the final system. In all cases the remnant's centre is identified using the most bound particle, which agrees very well with the centre of mass recursively calculated using smaller spherical regions.

The radial merger produces a prolate axisymmetric system with axial ratios  $a:b:c = 2:1:1$  where  $a$ ,  $b$  and  $c$  are the long, intermediate and short axis, respectively. We compute the shapes of our DM haloes from the principal moments of inertia using the iterative technique described in (Katz 1991). The dimensionless spin parameter of the remnant, which is defined by

$$\lambda = \frac{J|E|^{\frac{1}{2}}}{GM^{\frac{5}{2}}} \quad (4)$$

where  $J$ ,  $E$  and  $M$  are the angular momentum, the total energy and the total mass respectively, corresponds to  $\lambda = 0$  as expected in a radial merger.

In a second experiment we again start with the two spherical haloes separated by  $r_{\text{sep}} = 300$  kpc, but we give one halo a transverse velocity equal to the circular velocity of the combined model at that distance,  $v_{\text{rel}} = 240$  km s $^{-1}$ . The circular orbit merger produces an oblate halo with axial ratios  $a:b:c = 2:2:1$ . Haloes with any amount of triaxiality between these values could be created by using unequal mass mergers or mergers with less or more angular momentum. The spin parameter of the final system is  $\lambda = 0.1$ . It is interesting to note that with these experiments we have been able to reproduce most of the distribution of  $\lambda$  as seen in cosmological  $N$ -body simulations (e.g., Warren et al. 1992; Lemson & Kauffmann 1999). Figure 1 shows the density profile of the initial spherical model and of the prolate and oblate haloes. We also note that the slope of the central density profile remains unchanged in agreement with recent results from high-resolution collisionless  $N$ -body simulations of major mergers of cuspy DM haloes (Boylan-Kolchin & Ma 2003). In Figure 2 we show the central circular velocity curves of the initial model and the final prolate and oblate haloes. These have all been scaled by the same factor in radius and velocity such that all the curves have the same peak circular velocity. The prolate halo has a nearly identical concentration to the initial spherical model, but the oblate halo is nearly a factor of two less concentrated.

In order to create haloes with higher amounts of flattening it is necessary to merge together the products of the first set of simulations. Merging two prolate haloes along the long axis, again at a velocity such that the system is just bound produces a  $a:b:c = 3:1:1$  remnant, whilst merging two oblate haloes in the plane of the long axis, but counter-rotating, results in a further flattened system with axial ratios  $a:b:c = 3:3:1$  and no net angular momentum, but with particles streaming in opposite directions. Figure 3 shows two contoured images of the latter oblate halo viewed projected along the short and long axis, respectively.

### 3 TIDAL EVOLUTION OF TRIAXIAL SUBHALOES

Numerical investigations of the tidal stripping and mass loss of substructure haloes in CDM models have previously been restricted to spherical systems with isotropic velocity dispersion ten-

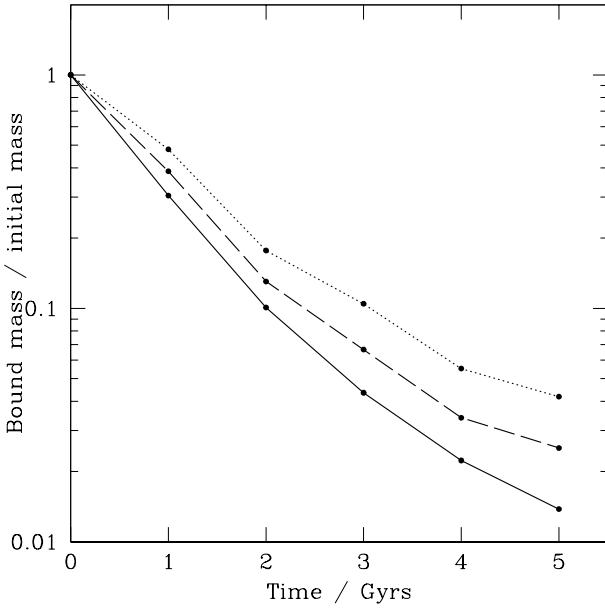


**Figure 4.** The rate of tidal mass loss over a period of 5 Gyr ( $\sim 2$  orbital periods) for the initial spherical model (dotted line), the  $a:b:c = 3:1:1$  prolate model (solid curve) and the  $a:b:c = 3:3:1$  oblate model (dashed curve). The prolate halo experiences much more efficient tidal stripping than both the spherical and oblate halo on the same external tidal field and orbit owing to the orbital distribution of particles supporting its shape.

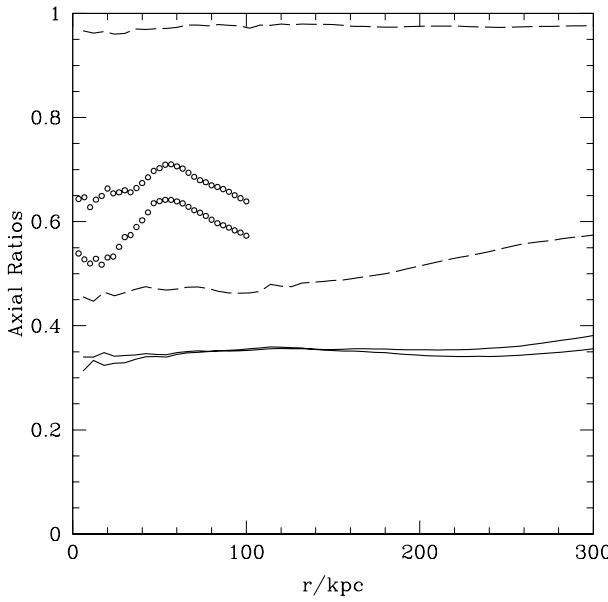


**Figure 5.** The axial ratios as a function of radius for the prolate (solid lines) and oblate (dashed lines) 3:1 haloes. The open circles show the axial ratios of the same prolate model after orbiting for 5 Gyr within a deeper potential.

sors (e.g., Taffoni et al. 2003; Hayashi et al. 2003). The results of these simulations are also incorporated into semi-analytic models which attempt to follow the tidal evolution of orbiting subhaloes. However, the shapes and velocity dispersion tensors of haloes in cosmological simulations have been studied by many authors (e.g., Warren et al. 1992; Cole & Lacey 1996; Thomas et al. 1998; Colín, Klypin & Kravtsov 2000; Bullock 2002) and they ex-

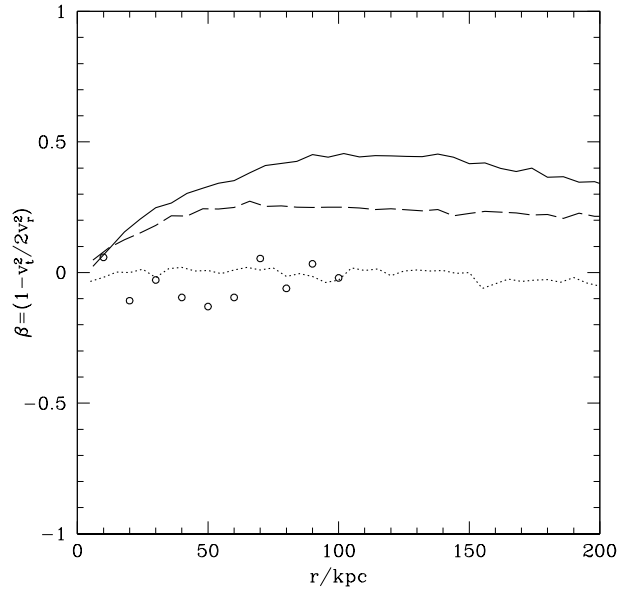


**Figure 6.** The anisotropy parameter  $\beta$  as a function of radius for the prolate halo model (solid line), oblate halo (dashed line) and initial conditions (isotropic spherical halo, dotted line). The open symbols show the anisotropy parameter for the prolate halo after orbiting for 5 Gyr within a deeper potential.

hibit a significant departure from spherical symmetry and isotropy. It is interesting to investigate if the response of a spherical subhalo to an imposed tidal field is the same as that of a triaxial subhalo.

KMM compared the resilience to tidal forces of two identical self-consistent NFW satellites on the same external tidal field and orbit, but constructed with different velocity dispersion tensors. Identifying the bound mass as function of time, these authors demonstrated that the satellite with a radially anisotropic velocity dispersion (Osipkov 1979; Merritt 1985) experiences much more efficient mass loss than its isotropic counterpart. This is due to the fact that particles on more radial orbits spend on average more time at larger radii and are therefore more easily stripped by the external field.

Here we expand on the previous result and show that similar differences are obtained when one considers the tidal evolution of spherical and triaxial haloes as they orbit within a deeper potential. We compare results of the 3:1 prolate and oblate haloes and the initial isotropic spherical halo used to create these models. The density profile of the spherical model is scaled by a factor of four in mass to preserve the same spherically averaged density profile as the prolate halo. Each halo is then placed on an identical orbit within a static cored isothermal potential such that the ratio of host to satellite halo circular velocities is  $v_{\text{host}}/v_{\text{sat}} = 10:1$  and the apocentric to pericentric radii is  $r_{\text{apo}}/r_{\text{per}} = 4:1$ . The satellite begins at apocentre which is set equal to the virial radius. This allows the satellite-host system to be rescaled to any galactic or cluster system. The imposed potential is reasonably soft since we use a core radius equal to half the pericentric radius. Significantly higher rates of mass loss may be expected in a more cuspy potential, however here we aim to explore the slow tidal loss of mass rather than mass loss due to strong tidal shocks. In a forthcoming paper we will give an analytical model for the rate of mass loss as a function of host potential, orbit and subhalo structure and shape (Kazantzidis et al. 2003, in preparation).

In Figure 4 we perform a comparison of the tidal evolution of

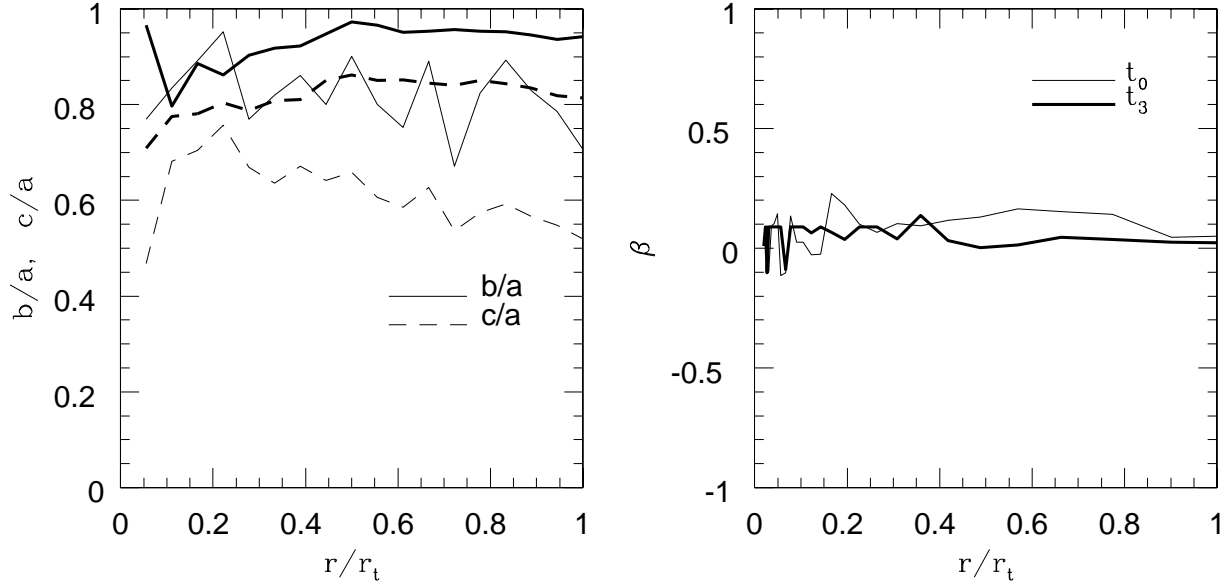


**Figure 7.** Structural and kinematic properties of one subhalo in our highest resolution cosmological run (R12) resolved with more than  $2 \times 10^5$  particles. Left: The axial ratios  $b/a$  and  $c/a$  as a function of radius from the subhalo's centre. Right: The anisotropy parameter  $\beta$  as a function of radius. In both cases, the thin lines correspond to measurements of the subhalo's properties just before entering the primary halo, whereas the thick lines correspond to its third pericentre passage. The subhalo becomes more spherical and isotropic as a result of the tides. Note that the radius of the subhalo is given in units of  $r_t$ , where  $r_t$  is its tidal radius after the third pericentre passage.

each of these three models by identifying the bound mass as a function of time using the publicly available group finder SKID<sup>1</sup> (Stadel 2001). The prolate halo experiences mass loss at a much higher rate than both the spherical and oblate ones. In Figures 5 and 6 we show the change in the shape and in the anisotropy parameter  $\beta$  of our models. The prolate halo becomes more spherical due to the tidal removal of particles on radial orbits that are supporting the shape of the system. In addition, after 5 Gyr of orbital evolution the velocity dispersion tensor of the prolate halo has significantly changed and now is nearly isotropic.

It is interesting to study the evolution of shape and anisotropy for haloes in a CDM simulation that enter into a deeper potential. This is important when we want to model the orbits of stars in satellite galaxies or the effect of subhaloes on lense models. Here we analyse subhaloes from a high resolution  $\Lambda$ CDM cluster simulation (Diemand, Moore & Stadel 2003, in preparation). The initial conditions are generated with the GRAFIC2 package (Bertschinger 2001). We start with a  $300^3$  particle cubic grid with a comoving cube size of 300 Mpc (particle mass  $m_p = 3.7 \times 10^{10} M_\odot$ ). We trace back and refine a cluster region region by a factor of 12 in length and 1728 in mass, so that the mass resolution is  $m_p = 2.14 \times 10^7 M_\odot$ . The softening length is comoving from the start of the simulation ( $z \simeq 40$ ) to  $z = 9$ . From  $z = 9$  until present, we use a physical softening length of  $1.05 \times 10^{-3} r_{\text{vir, parent}}$ . At  $z = 0$  the refined cluster contains  $1.4 \times 10^7$  particles (R12) and we select a relatively massive subhalo which is resolved with more than  $2 \times 10^5$  particles.

Figure 7 shows the axial ratios  $b/a$  and  $c/a$  (left panel) and the anisotropy parameter  $\beta$  (right panel) as a function of radius for this object. The thin lines correspond to the subhalo just before entering its host, whereas the thick lines correspond to the subhalo's third pericentre passage. Note that the radius of the subhalo is given

in units of  $r_t$ , where  $r_t$  is its tidal radius after the third pericentre passage. Figure 7 confirms that subhaloes become more spherical and their velocity distribution more isotropic owing to tidal effects. We then compare the mean axial ratios of field haloes versus subhaloes in the same simulation. On average we find that subhaloes have axial ratios that are 30% larger (more spherical) than field haloes.

#### 4 CONCLUSIONS

We have presented a method for constructing cuspy axisymmetric and triaxial  $N$ -body haloes based on merging isotropic equilibrium spherical haloes with varying amounts of angular momentum. In particular, we found that radial mergers produce prolate systems, whilst mergers on circular orbits produce oblate systems. This technique has the benefit that it is based on the way in which haloes obtain their triaxiality in cosmological simulations, therefore the anisotropy distributions and angular momentum of haloes are well motivated.

Mergers between similar equilibrium spherical haloes at high resolution show that the resulting halo has the same density profile, independent of the angular momentum of the merger. This has two implications: (i) the density profile of the triaxial halo can be set by the choice of the density profiles of the progenitor haloes and (ii) similar mass mergers can not dramatically re-arrange the central density structure of DM haloes, albeit oblate haloes (high angular momentum merger remnants) have concentrations up to a factor of two lower than prolate haloes (low angular momentum merger remnants). This may explain the entire scatter in the distribution of halo concentrations from cosmological simulations (Bullock et al. 2001; Eke et al. 2001; Wechsler et al. 2002). It may also be the case that the least concentrated haloes host the low surface brightness discs since these galaxies may form in high angular momentum oblate haloes. These galaxies generally require low values of the concen-

<sup>1</sup> <http://www-hpcc.astro.washington.edu/tools/skid.html>

tration when fit to cuspy halo models (e.g., McGaugh & de Blok 1998; van den Bosch et al. 2000; de Blok et al. 2001; Swaters et al. 2003).

As an application we considered the tidal evolution of triaxial subhaloes orbiting within deeper potentials. Haloes with identical spherically averaged density profiles and on identical orbits evolve self-similarly with time. Spherical haloes with isotropic velocity dispersion tensors suffer significantly less mass loss than radially anisotropic prolate ones. The latter is simply due to the fact that particles on radial orbits are easily stripped which also results in subhaloes becoming more spherical. In general, the subhaloes become more spherical and their velocity distribution more isotropic owing to tidal effects. This result has been confirmed by investigating the response to tides of both isolated satellite haloes orbiting within a static host potential and substructure haloes in the time dependent cosmological tidal field. We find that subhaloes in a cosmological simulation of a cluster are on average 30% rounder than their field counterparts. Galaxy subhaloes should be even closer to spherical since they spend longer being reshaped by the host potential.

Our more realistic modelling of DM haloes is important for studies of the weak and strong lensing statistics attempting to distinguish between competing cosmological models, the structural evolution and mass loss from substructure, the formation of tidal streams or the sizes of satellite haloes in galaxies and clusters. These results may also be important to incorporate within semi-analytic models that attempt to model the distribution of satellites in DM haloes. CDM haloes are generally radially anisotropic therefore they lose mass and are disrupted more quickly than the isotropic systems that have been generically considered in previous studies. This may explain why semi-analytic models predict far more substructures than found in high resolution numerical studies (e.g., Zentner & Bullock 2003, James Taylor private communication).

## ACKNOWLEDGMENTS

It is a pleasure to thank Victor Debattista and Lucio Mayer for useful discussions. BM thanks Priyamvada Natarajan for organising the Yale Cosmology Workshop “The Shapes of Galaxies and Their Dark Matter Haloes” (2001) which motivated some of this work and also apologises for not writing up the conference proceedings. The numerical simulations were carried out on the zBox (<http://www-theorie.physik.unizh.ch/~stadel/>). Initial conditions for the cosmological simulations were generated at the Swiss Center for Scientific Computing (SCSC) at Manno.

## REFERENCES

Barnes J. E., Efstathiou G., 1987, *ApJ*, 319, 575  
 Bartelmann M., Steinmetz M., Weiss, A., 1995, *A&A*, 297, 1  
 Bertschinger E., 2001, *ApJS*, 137, 1  
 Boily C. M., Kroupa P., Peñarrubia-Garrido J., 2001, *NewA*, 6, 27  
 Boylan-Kolchin M., Ma, C.-P., 2003, submitted to *MNRAS* (astro-ph/0309243)  
 Bullock J. S., Kolatt T. S., Sigad Y., Somerville R. S., Kravtsov A. V., Klypin A. A., Primack J. R., Dekel, A., 2001, *MNRAS*, 321, 559  
 Bullock J. S., 2002, in *The Shapes of Galaxies and Their Dark Haloes*, ed. P. Natarajan (Singapore: World Scientific), p. 109  
 Buote D. A., Canizares C. R., 1994, *ApJ*, 427, 86  
 Buote D. A., Canizares C. R., 1996, *ApJ*, 457, 177  
 Buote D. A., Canizares C. R., 1998, in *ASP Conf. Ser.* 136, *Galactic Haloes*, ed. D. Zaritsky (San Francisco: ASP), p. 289  
 Buote D. A., Jeltema T. E., Canizares C. R., Garmire G. P., 2002, *ApJ*, 577, 183  
 Cole S., Lacey, C., 1996, *MNRAS*, 281, 716  
 Colín P., Klypin A. A., Kravtsov A. V., 2000, *ApJ*, 539, 561  
 de Blok W. J. G., McGaugh S. S., Bosma A., Rubin, V. C., 2001, *ApJ*, 552, L23  
 Dubinski J., Carlberg R.G., 1991, *ApJ*, 378, 496  
 Eddington A. S., 1916, *MNRAS*, 76, 572  
 Eke V. R., Navarro J. F., Steinmetz M., 2001, *ApJ*, 554, 114  
 Franx M., van Gorkom J. H., de Zeeuw, T., 1994, *ApJ*, 436, 642  
 Frenk C. S., White S. D. M., Davis M., Efstathiou G., 1988, *ApJ*, 327, 507  
 Hayashi E., Navarro J. F., Taylor J. E., Stadel J., Quinn T., 2003, *ApJ*, 584, 541  
 Helmi A., 2003, submitted to *MNRAS* (astro-ph/0309579)  
 Hernquist L., 1990, *ApJ*, 356, 359  
 Hernquist L., 1993, *ApJS*, 86, 389  
 Holley-Bockelmann K., Mihos J. C., Sigurdsson S., Hernquist L., 2001, *ApJ*, 549, 862  
 Ibata R., Lewis G. F., Irwin M., Totten E., Quinn T., 2001, *ApJ*, 551, 294  
 Iodice E., Arnaboldi M., Bournaud F., Combes F., Sparke L. S., van Driel W., Capaccioli M., 2003, *ApJ*, 585, 730  
 Jing Y. P., Suto Y., 2002, *ApJ*, 574, 538  
 Johnston K. V., Zhao H., Spergel D. N., Hernquist L., 1999, *ApJ*, 512, L109  
 Katz N., 1991, *ApJ*, 368, 325  
 Kazantzidis S., Magorrian J., Moore B., 2003, accepted by *ApJ* (astro-ph/0309517)  
 Kochanek C.S., 1995, *ApJ*, 445, 559  
 Koopmans L. V. E., de Bruyn A. G., Jackson N., 1998, *MNRAS*, 295, 534  
 Kuijken K., Tremaine S., 1994, *ApJ*, 421, 178  
 Lemson G., Kauffmann G., 1999, *MNRAS*, 302, 111  
 Majewski S., Skrutskie M.F., Weinberg M.D., Ostheimer J.C., 2003, submitted to *ApJ* (astro-ph/0304198)  
 Mayer L., Moore B., Quinn T., Governato F., Stadel, J., 2002, *MNRAS*, 336, 119  
 McGaugh S. S., de Blok W. J. G., 1998, *ApJ*, 499, 41  
 Merrifield M. R., 2002, in *The Shapes of Galaxies and Their Dark Haloes*, ed. P. Natarajan (Singapore: World Scientific), p. 170  
 Merritt D., 1985, *AJ*, 90, 1027  
 Moore B., Calzáneo-Roldán C., Stadel J., Quinn T., Lake G., Sebastianiano G., Governato F., 2001, *Phys. Rev. D*, 64, 063508  
 Navarro J. F., Frenk C. S., White S. D. M., 1996, *ApJ*, 462, 563  
 Oguri M., Lee J., Suto Y., 2003, accepted by *ApJ* (astro-ph/0306102)  
 Osipkov L. P., 1979, *Soviet Astron. Lett.*, 5, 42  
 Sackett P. D., Sparke L. S., 1990, *ApJ*, 361, 408  
 Schoenmakers R. H. M., Franx M., de Zeeuw P. T., 1997, *MNRAS*, 292, 349  
 Schwarzschild M., 1979, *ApJ*, 232, 236  
 Schweizer F., Whitmore B. C., Rubin V. C., 1983, *AJ*, 88, 909  
 Sparke L. S., 2002, in *The Shapes of Galaxies and Their Dark Haloes*, ed. P. Natarajan (Singapore: World Scientific), p. 178  
 Stadel J., 2001, PhD thesis, Univ. Washington  
 Swaters R. A., Madore B. F., van den Bosch F. C., Balcells, M., 2003, *ApJ*, 583, 732

Taffoni G., Mayer L., Colpi M., Governato F. 2003, MNRAS, 341,  
434

Thomas P. A. et al. , 1998, MNRAS, 296, 1061

van den Bosch F. C., Robertson B. E., Dalcanton J. J., de Blok W.  
J. G., 2000, AJ, 119, 1579

Vitvitska M., Klypin A. A., Kravtsov A. V., Wechsler R. H., Pri-  
mack J. R., Bullock J. S., 2002, ApJ, 581, 799

Warren M. S., Quinn P. J., Salmon J. K., Zurek W. H., 1992, ApJ,  
399, 405

Wechsler R. H., Bullock J. S., Primack J. R., Kravtsov A. V.,  
Dekel A., 2002, ApJ, 568, 52

Zentner A. R., Bullock J. S., 2003, accepted by ApJ  
(astro-ph/0304292)

This paper has been typeset from a  $\text{\TeX}$ /  $\text{\LaTeX}$  file prepared by the  
author.